Metastable phase-separated droplet generation and long-time DNA enrichment by laser-induced Soret effect

Mika Kobayashi*, Yoshihiro Minagawa, and Hiroyuki Noji*

Department of Applied Chemistry, Graduate School of Engineering University of Tokyo, Tokyo 113-8656, Japan

(Dated: December 2, 2024)

*Corresponding author. E-mail: kobayashi.phys@gmail.com; hnoji@g.ecc.u-tokyo.ac.jp

Abstract

Spatiotemporally controlled laser-induced phase separation (LIPS) offers unique research avenues and has a potential for biological and biomedical applications. However, LIPS conditions often have drawbacks for practical use, which limit their applications. For instance, LIPS droplets are tentative and diminish after the laser is terminated. Here, we developed a novel LIPS method using laser-induced Soret effect with a simple setup to solve these problems. We generate liquid-liquid phase-separated (LLPS) droplets using LIPS in an aqueous two-phase system (ATPS) of dextran (DEX) and polyethylene glycol (PEG). When DEX-rich droplets were generated in the DEX/PEG mix on the phase boundary, the droplets showed unprecedently high longevity; the DEX droplets were retained over 48 h. This counterintuitive behavior suggests that the droplet is in an unknown metastable state. By exploiting the capability of DEX-rich droplets to enrich nucleic acid polymers, we achieved stable DNA enrichment in LIPS DEX droplets with a high enrichment factor of 1400 ± 400. Further, we patterned DNA-carrying DEX-rich droplets into a designed structure to demonstrate the stability and spatiotemporal controllability of DEX-rich droplet formation. This is the first report for LIPS droplet generation in a DEX/PEG system with flexible conditions for the usage of LIPS droplets, opening new avenues for biological and medical applications of LIPS.

Keywords: LLPS, laser-induced phase separation, droplet kinetics, DNA enrichment, thermophoresis

Liquid-liquid phase separation (LLPS) attracts large interests in biological sciences since the recent findings that phase separation plays important roles in a wide variety of biomolecular systems(1–4). In addition to biological droplets, the ATPS (aqueous two-phase system) of Dextran (DEX) and polyethylene glycol (PEG) also draws a large attention because ATPS of DEX/PEG can enrich some of biomolecules in DEX-rich phase(5–8) while these polymers are chemically and biologically inert and thereby they show fine biocompatibility. In particular, DEX-rich droplets in DEX/PEG ATPS have been reported to well enrich DNA molecules(9). Other biomolecules such as RNA and proteins are also reported to have enriched in the DEX-rich phase(10, 11). For these reasons, DEX/PEG ATPS was utilized in microchemical/biological systems for efficient DNA and protein enrichment(8, 12) or in artificial cell models to enrich biomolecules and/or enhance biomolecular reactions(11, 13–15). Thus, spatiotemporal control of LLPS including DEX/PEG ATPS under the microscope is of great importance for biological applications.

Laser-induced phase separation (LIPS) is a method to generate LLPS droplets in a controlled manner and it has been investigated in several systems(16–27). Local heating upon laser irradiation to LCST (lower critical solution temperature) systems is a simple LIPS method(19) where droplets are created when the heated region satisfies the two-phase condition. However, the generation temperature for the LIPS in LCST systems is limited by the phase diagram and generally it requires high generation temperature which is not applicable in biological experiments. Especially, it is difficult to keep precise temperature control for biological reactions. In the case of DEX/PEG systems, there are some systems which show LCST(28). In principle, LIPS in those systems should be possible but LIPS DEX droplet generation has never been reported so far. This would be partly because of the above reasons.

Another approach for LIPS is to use the Soret effect (thermophoresis), which is a non-equilibrium phenomenon wherein a concentration gradient is formed under a temperature gradient(29). In this case, local concentration is modulated by temperature gradient, but temperature does not directly

drive phase separation. This means that the generation temperature is basically not limited by the phase diagram. LIPS by the Soret effect can be conducted at a desired temperature if the appropriate concentration gradient is formed. The concentration gradient of a molecule induced by the Soret effect, ∇c, is described as

$$\nabla c = -S_T\, c(1 - c)\, \nabla T,$$

where c, ∇T, and S_T represent the molecular fraction, temperature gradient, and ratio of the thermal mass diffusion coefficient (D_T) to the mutual mass diffusion coefficient (D), respectively; $S_T = D_T/D$. The value of S_T ranges from 10^{-5} to 10^{-1} (30). Whether a molecule accumulates ($S_T < 0$) or is excluded ($S_T > 0$) along a temperature gradient depends on its species and its combination with other molecules in the mixture(31). On the other hand, the concentration gradient generated by the Soret effect is generally not sufficient to induce phase separation. There are, therefore, only a few reports on LIPS using the Soret effect. Delville et al. demonstrated LIPS in a quaternary micellar system because the required concentration change was sufficiently small to achieve phase separation(16, 17). Voit et al. studied thermal patterning on a polymer blend using a focused laser beam and modulated phase separation near the critical point where the Soret coefficient diverges(21, 22).

Another drawback of LIPS so far is that LIPS droplets prepared using these methods are ephemeral and disappear after the termination of laser irradiation because the droplets are formed under non-equilibrium conditions in a stable single phase. The duration of the LIPS droplets is basically determined by the diffusion of molecules. In previous reports on LIPS experiments with binary mixtures, LIPS droplets disappeared within tens of minutes(21, 25). Thus, LIPS droplets are principally unstable and revert to the miscible solution state after laser induction(21, 25), which limits its range of application.

In this study, we aimed to develop a novel LIPS methodology for the generation of phase-separated DEX-rich droplets in a DEX/PEG system by use of the laser-induced Soret effect. DEX has a unique feature; this polymer exhibits a negative Soret coefficient, $S_T < 0$(31); DEX molecules accumulate to

the hot region along the temperature gradient. Thus, the negative S_T of DEX is, in principle, suitable for LIPS with the Soret effect. We developed a local heating system in which an infrared laser spot was introduced on a coverslip coated with a semiconductor which absorbs the infrared light and produces heat. The local heating produced a temperature gradient, which resulted in the local condensation of DEX via the Soret effect. The laser-induced Soret effect successfully triggered the formation of DEX-rich droplets. We discovered that the generated droplets were extraordinarily stable; the droplets were retained for over 48 h. It was also found that the DEX-rich droplets enriched DNA molecules by a factor of 1400. Finally, we demonstrated the patterning of DNA-containing droplets along the defined structures, by exploiting the controllability, longevity and capability for DNA enrichment of the LIPS-induced DEX-rich droplet.

LIPS droplet generation by laser-induced Soret effect

We produced LIPS droplets in a miscible mixture of DEX ($Mw = 4.5\text{–}6.5 \times 10^5$) and PEG ($Mw = 3.5 \times 10^4$). A phase diagram of the DEX/PEG system is illustrated in Fig. 1a. It does not change within the experimental temperature range of 293–363 K. Therefore, heating by laser irradiation did not directly affect the phase of the DEX/PEG system (See Methods). We performed experiments on a DEX/PEG mix on the coexisting curve, which is the phase boundary between single- and two-phase states, with the expectation that the system would inevitably enter the two-phase region by the small change in concentration induced by the Soret effect. The DEX/PEG mixture on the coexisting curve was prepared experimentally as follows; at first, a DEX/PEG was prepared at an initial composition in the two-phase region —DEX at 6 wt.% and PEG at 2.6 wt.% (open circles in Fig. 1a). The DEX/PEG mixture was equilibrated to form macroscopic two phases and complete phase separation, as shown in the photograph in Fig. 1a. Each phase obtained by the preparation should be exactly on the phase boundary because it is an equilibrium phase. The DEX/PEG compositions of the upper PEG-rich phase and the lower DEX-rich phase are estimated from the

101 fluorescent intensity of the spiked, fluorescently labelled DEX and PEG (Fig. 1a), respectively. The
102 compositions were consistent with those reported in a previous study(32). The upper PEG-rich phase
103 solution was used in subsequent experiments to induce DEX-rich droplet generation by LIPS.

104 Local heating was performed under a microscope using an infrared (IR) laser. Figure 1b illustrates
105 a schematic of the experimental setup. A temperature gradient was generated at the laser focus point,
106 where the IR laser light was absorbed by the ITO coat on a coverslip of a sample cell. The schematic
107 of DEX-rich droplet generation by LIPS is shown in Fig. 1c. The temperature gradient produced upon
108 the laser irradiation attracts DEX molecules via the Soret effect. The temperature at the heating spot
109 during laser irradiation was estimated to be +10 K from the surrounding medium, generating a
110 temperature gradient of 0.1 K/μm (*SI Appendix*, section 1). Subsequently, a DEX-rich droplet phase
111 appeared at the focal point of the IR laser.

112 Figure 1d illustrates time-lapsed images of the droplet-generation process (See also *SI Appendix*,
113 Movie 1). When the laser irradiation was initiated, the growth of the dark domain in the phase contrast
114 images was observed, as well as the growth of a fluorescence spot in the fluorescence images. After
115 the irradiation time for 10 min, the laser was switched off. Then, the small droplets suddenly appeared
116 around the main droplet (see phase-contrast images at 10 or 60 s after laser termination in Fig. 1d).
117 These satellite droplets gradually coalesced into the main droplet. The droplet interface was not clear
118 during laser irradiation, and it became sharp after laser termination. It is likely that the active mass
119 transport of DEX by the laser-induced Soret effect perturbed the formation of a stable interface. We
120 also examined LIPS using an ITO-free glass substrate. DEX accumulation and droplet formation were
121 not observed (*SI Appendix*, section 2), confirming that droplet generation was not induced by the
122 radiation pressure or electromagnetic force of the laser, but by local heating, which caused the Soret
123 effect. We confirmed that the temperature of the generated droplet can be changed after the laser is
124 switched off (*SI Appendix*, section 3).

125 When the DEX/PEG mix was prepared at concentrations below the coexisting curve (blue circle

126 in the phase diagram in Fig. 1a), laser irradiation failed to form a droplet, although DEX condensed
127 (Fig. 1e). When the irradiation was terminated, the accumulated DEX molecules diffused within
128 minutes. This means we need an initial sample very close to the coexisting curve for LIPS using the
129 Soret effect as more investigated below.
130

131 **Longevity of LIPS droplet**

132 The generated DEX droplets exhibited remarkable longevity. Figure 2a shows a representative
133 series of time lapsed images for 2 days. Figure 2b exhibits the time course of the diameter of the
134 droplet shown in Fig. 2a. Initially, the diameter was approximately 7 μm. After the initial shrinkage
135 process of 1–2 h, the droplet size reached a steady value of approximately 3 μm. Figure 2c illustrates
136 the diameters of the droplets generated under the same experimental condition plotted as a function
137 of the laser irradiation time t_{IR}. The initial diameter ranged from 6–12 μm, and the final diameter was
138 1–3 μm. Neither the initial nor the final diameter did not show a clear t_{IR}-dependence. This suggests
139 that DEX condensation by the laser-induced Soret effect plateaued within 5 min of irradiation.

140 We investigated the relationship between the droplet longevity and the initial composition of
141 DEX/PEG mixture. In particular, we asked how stable the generated droplets are when the initial
142 concentrations of DEX and PEG are below the coexisting curve (inset of Fig. 2d). For this purpose,
143 we prepared DEX/PEG mixtures by diluting the PEG-rich phase taken from DEX/PEG ATPS
144 solution, which systematically changed the distance from the coexisting curve (inset of Fig 2d). When
145 the DEX/PEG mix was prepared at a dilution factor of 0.9 (pink triangle in the inset of Fig. 2d), LIPS
146 droplets were once generated, however, they disappeared within 30 min (pink triangles in Fig. 2d).
147 The droplets prepared in diluted mix shrank significantly faster than that without dilution. When the
148 DEX/PEG mix was more diluted; the dilution factor was less than 0.9 (blue crosses in the inset of
149 Fig. 2d), and no droplet formation was observed. Figure 2e shows the time-courses of the droplet
150 diameter for the samples with the dilution factors from 1 and 0.9. We analyzed the initial linear regime

151 using linear fitting to estimate the initial speed of droplet shrinkage, v_0. The results are shown in Fig.
152 2f. The rate of shrinkage, v_0 decreases systematically as the dilution factor approaches 1 (no dilution:
153 on the coexisting curve). This suggests that the driving force to revert the droplet to the original
154 miscible state decreases, when the composition of DEX/PEG mix approaches the coexisting curve.
155 The relationship between the initial composition in the phase diagram and the appearance of longevity
156 is schematically explained in Fig. 2 g and h. These findings confirm that the DEX/PEG mix
157 composition has to be quite close or on the coexisting curve for stable DEX droplet generation.
158

159 **DNA enrichment in LIPS droplet**

160 We attempted DNA enrichment in LIPS DEX droplets by exploiting the capability of DEX-rich
161 droplets to enrich DNA molecules(9). The concept of our experiment is schematically illustrated in
162 Fig. 3a; the longevity of DEX-rich LIPS droplets is expected to achieve stable DNA enrichment. First,
163 we examined the possibility of DNA enrichment in LIPS droplets. The PEG-rich phase solution for
164 LIPS was prepared with λ-DNA (48,502 bps) through the protocol as same as the above experiments.
165 The DNA concentration in the prepared PEG-rich solution was 70 pg/μL (see Methods and *SI*
166 *Appendix*, section 4). We conducted LIPS with DNA-containing PEG-rich solution as same as above.
167 Fig. 3b shows the images of a LIPS DEX droplet generated upon laser irradiation for 5 min. The
168 fluorescence image of the DNA intercalator reveals the enrichment of DNA in the LIPS droplet. The
169 droplets with enriched DNA were as stable as droplets prepared without DNA. After initial shrinkage,
170 the droplets retained a constant diameter over 24 h. The fluorescence signal from DNA was more
171 stable than that from DEX; the fluorescence signal of DNA in droplets was observed even after 18 h
172 (Fig. 3c), while the fluorescence signal of DEX became significantly darker compared with the initial
173 fluorescence signal (t = 0 h).

174 For more quantitative analysis on the concentration of DNA and DEX of the LIPS droplets, the
175 fluorescence intensity of the droplets was measured with confocal microscopy. This is because the

176 fluorescence images of the droplets in epifluorescence microscopy contained a considerable level of
177 background fluorescence intensity from the surrounding medium, hampering accurate measurement.
178 LIPS droplets were prepared on laser-equipped epifluorescence microscopy and subsequently
179 translated to confocal microscopy for time-evolution observation. Therefore, the confocal microscopy
180 observations were started several minutes after LIPS. However, as shown below, the time evolution
181 of the fluorescent signal of DNA/DEX in LIPS droplets exhibited significantly slower change, in the
182 order of tens of minutes. Thus, the delay caused by sample translation was neglected.

183 Figure 4a displays the representative time-lapsed images of the LIPS droplets visualized by
184 fluorescent DNA/DEX after laser irradiation for 12 min. The time course of droplet diameter is shown
185 in *SI Appendix*, Fig. S1a. It showed an exponential decay and converged to a finite value around 3
186 μm. The fluorescent intensity of DNA in the LIPS droplet showed a temporal rise around 51 min,
187 followed by decay. In contrast, the fluorescence intensity of DEX showed a simple monotonous decay.
188 We defined the enrichment factor of DNA, EF^{DNA} as the ratio of DNA concentration in a LIPS droplet
189 to that in the surrounding PEG-rich solution, $EF^{\mathrm{DNA}} = [\mathrm{DNA}]_{\mathrm{droplet}}/[\mathrm{DNA}]_{\mathrm{surrounding}}$. The DNA
190 concentration in droplets ranged from 50 to 200 ng/μL, while that of the surrounding PEG-rich phase
191 solution was 70 ± 10 pg/μL (see Methods and *SI Appendix*, section 4). The time evolution of EF^{DNA}
192 is illustrated in Fig. 4b. As observed in the time-lapsed images, EF^{DNA} initially showed a transient
193 rise to the maximum value around 50 min, followed by slow decay to a steady level. The statistical
194 analysis showed the mean values of the initial, maximum, and steady stages were 1200, 2000, 1400
195 (Fig. 4d). The individual data were plotted against the initial droplet diameter d_0 in *SI Appendix*, Fig.
196 S2a. Although the exact mechanism for the transient rise of EF^{DNA} is not clear, it is attributable to
197 condensation upon the droplet shrinkage (See *SI Appendix*, Fig. S1a). Time t_{max} when EF^{DNA} showed
198 its maximum is shown in *SI Appendix*, Fig. S3a. In some cases, there was no evident maxima (*SI*
199 *Appendix*, Fig. S3b).

200 The concentration ratio of DEX of the droplet to the surrounding solution, CR^{DEX} was estimated

201 as the fluorescence intensity ratio of the droplet to that in the surrounding PEG-rich solution, CR^{DEX}
202 = $[DEX]_{droplet}/[DEX]_{surrounding}$ (*SI Appendix*, section 4). Fig. 4c shows the time evolution of CR^{DEX}
203 that exhibited an exponential decay from approximately 6 to a plateau level, around 2 (Fig. 4c). The
204 trend of the DEX concentration decrease can be seen in the result of statistical analysis shown in Fig.
205 4e. The validity of the change is discussed in *SI Appendix*, section 5. The individual data were plotted
206 against the initial droplet diameter d_0 in *SI Appendix*, Fig. S2b. The timescale of the decay in CR^{DEX}
207 was similar to that of the diameter (*SI Appendix*, Fig. S4).
208 The presence of DNA did not show a significant effect on the behavior of the LIPS droplets. The
209 decay rate of the droplet diameter was the order of 10^1 min in both cases, w/ and w/o DNA (*SI*
210 *Appendix*, Fig. S1b). The initial value and the final value of CR^{DEX} were almost the same between w/
211 and w/o DNA shown in Fig. 4e.
212
213 **Comparison of LIPS droplet and spontaneous droplet**
214 We compared LIPS droplets with droplets formed by spontaneous phase separation. The
215 spontaneous droplets of the DEX-rich phase were prepared by agitation of the two-phase DEX/PEG
216 mix which is the same composition as that used in LIPS experiments and observed in confocal
217 microscopy (*SI Appendix*, section 6). The DNA enrichment factor EF^{DNA} and the DEX concentration
218 ratio CR^{DEX} of spontaneous droplets were compared with those of LIPS droplets in Figs. 5a and 5b,
219 respectively. The mean values of initial or final EF^{DNA} for LIPS droplets are 1200 and 1400 which
220 are higher than EF^{DNA} for spontaneous droplets, around 600 (Fig.5a). The distribution of EF^{DNA} for
221 LIPS droplets is wider than that of spontaneous ones. The mean values of initial or final CR^{DEX} for
222 LIPS droplets are 6.9 and 3.0 which are smaller than CR^{DEX} of spontaneous ones, 9.4 (Fig.5b).
223 For the direct comparison of LIPS droplets and spontaneous droplets, we conducted LIPS with
224 ATPS of DEX/PEG; the PEG-rich phase solution containing spontaneous DEX-rich droplets (Fig.
225 5c-f). LIPS droplets were generated as same as in the other experiments. The fluorescent intensity of

226 DNA in the LIPS droplet at $t = 7$ min after generation was higher than the spontaneous one by a factor
227 of 4.3. The intensity of DEX was lower than the spontaneous one by a factor of 0.7. Thus, the direct
228 comparison confirmed that LIPS droplets have higher EF^{DNA} and lower CR^{DEX} than those of
229 spontaneous droplets. These observations indicate that the property of LIPS droplets is not very far
230 from that of spontaneous phase separation, but different from it. In the PEG concentration in this
231 study, the Soret effect of DNA itself(33) could contribute to the mechanism for the higher EF^{DNA}
232 for LIPS droplets than that of spontaneous one(34, 35). If so, EF^{DNA} could increase further by
233 increasing t_{IR} up to the equilibrium of the Soret effect. Braun et al. demonstrated laser-induced DNA
234 enrichment using the Soret effect and convection although it is not a phase separating system(36).
235 The enriched DNA in their method diffused away after heating. In our case, convection is negligible
236 since local heating is achieved by heating the ITO surface at the bottom of the sample cell. Note that
237 we confirmed that the Soret effect of DNA itself is not the mechanism for the stable DNA enrichment
238 in LIPS droplets (*SI Appendix*, section 7).
239
240 **Composition of LIPS droplet**
241 The composition of LIPS droplets was estimated in confocal measurements by spiking
242 fluorescently labelled DEX and PEG in DEX/PEG mix (See Methods and *SI Appendix*, Fig. S5). The
243 initial and final DEX/PEG compositions of LIPS are plotted as the dotted and closed blue circles in
244 *SI Appendix*, Fig. S5d, respectively. These compositions were estimated from the mean values of
245 CR^{DEX} and CR^{PEG} at the initial state, i.e., just after LIPS: $t \sim 5$ min and after long-time incubation: $t \sim$
246 100 min (*SI Appendix*, Fig. S5a, b, c). The initial composition is close to the composition of the DEX-
247 rich phase in the spontaneous ATPS of DEX/PEG (red triangle in *SI Appendix*, Fig. S5d), while the
248 final composition is close to the PEG-rich phase (red circle in *SI Appendix*, Fig. S5d). This means
249 that the DEX/PEG composition of LIPS droplet gradually changes with time, approaching to the
250 composition of PEG-rich phase. However, as seen in the stable plateau of CR^{DEX} in Fig. 4c, the LIPS

251 droplet almost pauses the composition change to stay at a particular composition in the metastable
252 state.
253
254 **Patterning of LIPS droplets**
255 Finally, we attempted to demonstrate the controllability, reproducibility, and longevity of LIPS
256 droplets by patterning LIPS droplets in the presence of DNA along a designated structure. Multiple
257 LIPS droplets were generated at the defined position to draw a heart mark by laser irradiation for 5
258 min (*SI Appendix*, Movie 2). The time interval between each LIPS was 1 min and the distance between
259 droplets was approximately 50 μm. Fig. 6 shows the fluorescence image of DNA-containing LIPS
260 droplets, stained with the intercalator dye. The patterned LIPS droplets demonstrate not only the
261 controllability of LIPS but also that LIPS droplets do not interfere with the formation of neighbor
262 droplets under the present condition. More complicated patterning should be possible if our method
263 is combined with laser foci technique (37, 38). In preliminary experiments, we also found that it is
264 possible to translocate LIPS droplets by moving the laser focal point. Exploiting these phenomena,
265 the coalescence of two droplets was also demonstrated via manipulation (*SI Appendix*, Movie 3). This
266 demonstration confirms the fluidity of the LIPS droplets, stating that the longevity is not caused by
267 trivial processes such as gelation or other chemical reactions. We also observe the abrupt
268 disappearance of LIPS droplets by short laser irradiation (*SI Appendix*, Movie 4). Thus, the current
269 system allows for the microscopic handling of LIPS droplets: the patterning, translocation, fusion,
270 and clearance of the DEX-rich droplets, although the precise understanding of the mechanism for
271 these phenomena needs further studies.
272
273 **Discussion**
274 The most prominent finding of this study is the extraordinarily long-time stability of the LIPS
275 droplets which allows stable DNA enrichment. The generated droplets in our method are principally

276 non-equilibrium droplets because the initial state of the sample is a homogeneous single PEG-rich
277 phase. Intuitively, the droplets were expected to disappear, as observed in the LIPS experiments
278 conducted thus far(21, 25). However, the generated droplets did not vanish for a significantly long
279 time after the laser was disabled. We observed a distinct decrease in the diameter, indicating that the
280 system moved towards the original point on the coexisting curve. However, the shrinkage stopped at
281 a point before returning to the original homogenous PEG-rich phase. Resultantly, the DEX/PEG
282 composition of the droplets was close to but not exactly on the phase boundary (*SI Appendix*, Fig.
283 S5). These observations mean that LIPS droplets were stacked in a metastable state. The stable LIPS
284 droplets were also generated by using ATPS of DEX/PEG with different compositions, suggesting
285 the generality of the stable LIPS droplets. Regarding the metastability, it is also worth noting the
286 laser-induced disappearance of LIPS droplets (*SI Appendix*, Movie 4). The laser irradiation seems to
287 work as a perturbation to agitate the metastable droplets and the surrounding phase, and as a result,
288 the droplets returned into the most stable state of the homogeneous phase. Consistent with this
289 interpretation, spontaneously formed DEX-rich droplets in DEX/PEG ATPS which are stable in
290 nature were retained even after the laser irradiation (*SI Appendix*, Movie 5).

291 The initial condition of the sample on the phase boundary would be a key to the mechanism for
292 the longevity of LIPS droplets. For the system exactly on the phase boundary, the other coexisting
293 phase is energetically the same. This implies that, in principle, the system can shift towards both
294 directions. This can be a similar situation to the coexistence of the ice at 0 °C in water at 0 °C. There
295 should be competing effects between two equilibrium phases to which the system should go. The
296 initial speed of droplet shrinkage decreased when the system was approaching the coexisting curve
297 (Fig. 2f), suggesting that the driving force to cross the phase boundary to return toward the original
298 equilibrium in the one-phase region dramatically decreases and this causes the longevity as
299 schematically illustrated in Fig. 2g and h. On the other hand, this contention does not give full
300 explanation for the reason why the system has metastable states.

301 The present study indicates that there is an unknown mechanism which prevents the system from
302 crossing the phase boundary to return to the one-phase region. According to the classical nucleation
303 theory for phase separation, there is a critical radius R_c for droplet growth, for which the energy barrier
304 is determined by the interfacial energy and the bulk free energy of a droplet. While droplets of radius
305 smaller than R_c preferentially shrink, droplets show a stable growth when they occasionally reached
306 R_c(39). In the reverse process, it should be different from the same R_c, but there would be a similar
307 energy barrier for droplet shrinkage when the system crosses the phase boundary from the two-phase
308 region. That might be a mechanism for the remarkable longevity of the LIPS droplets. Of course, this
309 model would be too simplified. The exact understanding of the molecular mechanism for the
310 metastability of LIPS droplets needs future study.

311 In recent years, many studies reported that intracellular droplets of biomolecules, termed 'cell
312 biological droplets' play pivotal roles in biology(1–3, 40–42). Thereby, the physicochemistry of phase
313 separation systems attracts large attention not only in soft matter physics but also in chemical biology,
314 biophysics and molecular biology(43–45) . The metastable droplet generation mechanism in this
315 study might be related to the formation of stable cellular structures in protocells. It would be
316 interesting to apply our method to systems consisting of cell extract or living cell systems. The
317 DEX/PEG system investigated herein also attracts attention because the DEX-rich droplet is a model
318 system to build protocell or artificial cell systems(6). Our method can be utilized to produce cellular
319 structures in artificial cells or to the local formation of DNA origami structures. So far, we could not
320 keep both the LIPS droplet and the surrounding phase at the same temperature in principle, but the
321 present method enables us to do it. Our method has no limitation in generation temperature and the
322 temperature can be changed even after generation (*SI Appendix*, section 3), which provides a way to
323 develop new tools for biochemical reactions and digital bioassays such as digital PCR. Further, the
324 PEG-rich phase enables the enrichment of rare substances and their manipulation from its dilute
325 solution, which could be applied to drug delivery. We preliminarily confirmed that RNA could also

326 be enriched in the LIPS droplets. Proteins such as antibodies can be enriched in DEX-rich droplets,
327 in particular when they are tagged with dextran-binding domain (DBD)(8). Considering these, the
328 present LIPS method would be a technological basis for the microscopic manipulation of biological
329 molecules/systems by use of LIPS droplets as a carrier.

330 In summary, we succeeded in metastable LIPS droplet generation with unexpected longevity
331 which has never been observed before. The counterintuitive longevity is putting a fundamental
332 question to physics. It is also the first report of success in LIPS DEX droplet generation using the
333 DEX/PEG system and in LIPS DNA droplet generation which keeps fluidity. We achieved highly
334 stable DNA enrichment by a factor of thousands. The advantage of our system is its applicability to
335 a variety of biomolecules not only DNA and RNA but also proteins such as enzymes and antibodies
336 tagged with dextran-binding domain (DBD). We conducted the concentration-driven LIPS using the
337 Soret effect, which gave controllability of generation temperature. Simple setup by conventional
338 equipment gave accessibility for laboratory use. Those features widen the possibility of applications
339 of LIPS droplets in biological research. The properties of encapsulating substances accompanied by
340 phase separation, are important also in pharmaceuticals(46), medical science, and agricultural science.
341

342 **Materials and Methods**

343 **Materials.** We prepared a sample by mixing Dextran (DEX, Mw = 4.5 – 6.5 × 10^5, Sigma),
344 Polyethylene glycol (PEG, Mn = 3.5 × 10^4, Aldrich), λ-DNA (48,502 bp, Nippon Gene), and pure water.
345 To visualize and evaluate the concentration of polymers, we used TRITC-Dextran (Mw = 5.0 × 10^5,
346 Sigma) and FITC-PEG (Mw = 3.0 × 10^4, Creative PEG Works). DNA was visualized using an
347 intercalator (SYBR Gold; Invitrogen). DEX and PEG were dissolved in water at 20 wt.% as stock
348 solutions before mixing.

349 The phase diagram of the system is shown in Fig. 1a. We chose the system of the above molecular
350 weights of DEX and PEG because the temperature dependence of the phase diagram is negligible. This
351 means that our droplet generation is not induced by temperature-driven phase separation but by the
352 Soret effect. We confirmed this property experimentally by the fact that phase separation cannot be
353 induced by heating the bulk sample (see also *SI Appendix*, section 2). Note that the temperature effect to
354 phase separation in DEX/PEG system depends on the molecular weight of polymers and there are other
355 DEX/PEG systems which show clear temperature dependence for the lower molecular weight of DEX
356 and PEG(28, 47).

357 For the droplet-generation experiments, we first prepared a sample with an initial composition in
358 the two-phase region to experimentally obtain a sample on the coexisting curve. All components were
359 mechanically mixed using a conventional vortex mixer and centrifuged at 15,000 rpm (Eppendorf
360 Himac Technologies, CF18RS relative centrifugal force of 16,451.37*g*) for 20 min under temperature
361 control at 298 K. The upper PEG-rich phase (indicated by an arrow in Fig. 1a) produced from the
362 mixture was extracted and used as a sample. For the mixture of DEX 2.6 wt.% PEG 6 wt.% (open
363 circle in Fig. 1a), the composition of two separated phases after centrifugation estimated from the
364 fluorescent intensity of a dye (TRITC-DEX, FITC-PEG) using a microplate reader (Molecular
365 Devices, SpectraMax iD3) was DEX 0.7 wt.% and PEG 3.1wt.% for the upper PEG-rich phase and
366 DEX 8.4 wt.% and PEG 0.9 wt.% for the lower DEX-rich phase, where we assumed that the

concentration of the polymer with the dye was directly proportional to that of the dye-free polymer of the same type. The quantity of fluorescently labelled DEX varied from 0.02%–0.2% depending on the experiment. The concentrations in the text denote the total DEX concentration. The DNA concentration of each equilibrated phase was 70 pg/μL for the upper PEG-rich phase estimated by the confocal image of DNA, and 60 ng/μL for the lower DEX-rich phase estimated by spectroscopy (Thermo Scientific, NanoDrop 2000).

To observe the spontaneously forming droplets, we used a vortex mixer to agitate the solution for a few minutes. Subsequently, we used the upper PEG-rich phase containing DEX-rich droplets after waiting for a sufficient amount of time for sedimentation to reduce the number of droplets for 30 min.

Local heating experiments and microscopy. Local heating was performed under a microscope (Nikon Ti2E). An infrared (IR) laser with a wavelength of 1,064 nm was connected to the microscope and focused on the sample (Thorlabs; Diode laser 1064 nm, a laser power of 30 mW at the sample position). The sample was sandwiched between a cover glass and a glass plate with ITO (Indium Tin Oxide) coating (EHC. Co. Ltd.; ITO thickness = 20–40 nm, and resistance = 100 ohms). ITO absorbs light of wavelength 1,064 nm, which causes a temperature increase at the beam position. The sample thickness was controlled by a polyimide film with a thickness of 85 μm. The temperature of the sample cell was controlled at 298 ± 0.1 K by a temperature stage (Linkam PE120) with a Peltier module. For multiple-droplet generation, temperature control is necessary to prevent the temperature gradient caused by laser irradiation from influencing the droplets. The maximum temperature increase by local heating was approximately 10 K, which was estimated from the temperature dependence of fluorescence intensity of Rhodamine B solution in water (*SI Appendix*, section 1). The microscope images were captured using a CMOS camera (Andor Zyla).

For confocal microscopy, the droplets were generated using the local heating setup described above and they were observed under a confocal microscope (Leica Microsystems, SP-8). The glass

392 plate (thickness of 0.7 mm) with an ITO coating is greater than the working distance of the objective
393 lens (100X, N.A. 1.47) used in confocal microscopy. The sample cell was flipped, and the induced
394 droplets were observed from the bottom. For the simultaneous observation of induced and
395 spontaneous droplets, a glass plate (thickness 0.2 mm) with an ITO coating was used without flipping
396 over the plate. A white laser was used for excitation (488 nm for SYBR gold or FITC-PEG and 561
397 nm for TRITC-DEX), and the experiment was performed with the minimum number of acquisitions
398 to reduce the contribution of photobleaching. We did not perform 3D acquisition every time in a time-
399 course measurement and analyzed kinetics using the droplet diameter instead of droplet volume for
400 the same reason. Under this condition, the decrease in intensity caused by photobleaching can be
401 considered negligible (*SI Appendix*, section 5). The background light caused by the reflection of the
402 laser from the substrate was removed by notch filters and time-gated acquisition from 0.2 ns. The
403 time evolution was observed at room temperature (297 ± 0.5 K). The droplet diameter was estimated
404 by contour detection using commercial software (Image Pro Plus, Media Cybernetics). As the
405 obtained values could be underestimated, we set the error bar to ± 0.5 μm. For the non-linear fit
406 analysis of the droplet diameter, we added the initial droplet diameter after LIPS (t = 0) determined
407 from the phase contrast microscopy image to the time evolution of the droplet diameter observed by
408 confocal microscopy as the value d_0 at t = 0.

409 For the estimation of the composition of the LIPS droplets, we performed the LIPS droplet
410 generation experiments on the sample including fluorescently labelled DEX and PEG (TRITC-
411 Dextran (Mw = 5.0×10^5, Sigma) and FITC-PEG (Mw = 3.0×10^4, Creative PEG Works)). The
412 concentration ratios of DEX (CR^{DEX}) and PEG (CR^{PEG}) between the droplet and the surrounding phase
413 were determined as a fluorescent intensity ratio. They were converted to the concentration by
414 multiplying the concentration of the surrounding phase (0.7 wt.% for DEX, 3.1 wt.% for PEG).
415
416

Estimation of absolute DNA concentration. We determined the DNA concentration by comparison with the confocal data of DNA suspension in water with SYBR gold (See also *SI Appendix*, section 4). At a low concentration range below 100 pg/μL, DNA molecules are isolated and visible in confocal images because the full length of λ-DNA (48,502 bp) is approximately 16 μm. We counted the number of DNA molecules in several images and obtained the concentration dependence of the number per unit area (*SI Appendix*, Fig. S10). At the concentration range above 100 pg/μL, it becomes difficult to distinguish the isolated DNA molecules. We observed the confocal image of DNA suspensions in the same sample cell and other experimental conditions with that of the LIPS experiments. The concentration dependence of the average fluorescent intensity was measured and used to determine the absolute concentration of the LIPS droplets.

Acknowledgements

The authors thank Masao Doi for stimulating discussions on the mechanism of metastability. They thank Hajime Tanaka for helpful discussions on phase separation kinetics and his constant encouragement. They are grateful to Takahiro Muraoka for valuable discussions and his encouragement. They also thank Yutaro Ii for providing RNA samples, Shinichiro Kanatsuki for technical support of temperature control, and Kazutaka Irisawa for the optimization of ITO coating. This work was supported in part by Grant-in-Aid for Scientific Research (S; JP19H05624 to H.N.) and (C; 19K03763 to M.K.) from the Japan Society for the Promotion of Science (JSPS), and JST CREST, Japan (JPMJCR19S4 to H.N.), and the Kao Foundation for Arts and Sciences (Kao Crescent award to M.K.).

Author contributions

H.N. designed the project and supervised the study. M.K. performed the experiments and discovered the long-time presence of LIPS droplets. M.K. interpreted the physical mechanism underlying the phenomenon and analyzed the data. All authors discussed the results. M. K. and H. N. prepared the manuscript.

Competing interests

The authors declare no competing interests.

Correspondence and requests for materials should be addressed to

Hiroyuki Noji or Mika Kobayashi.

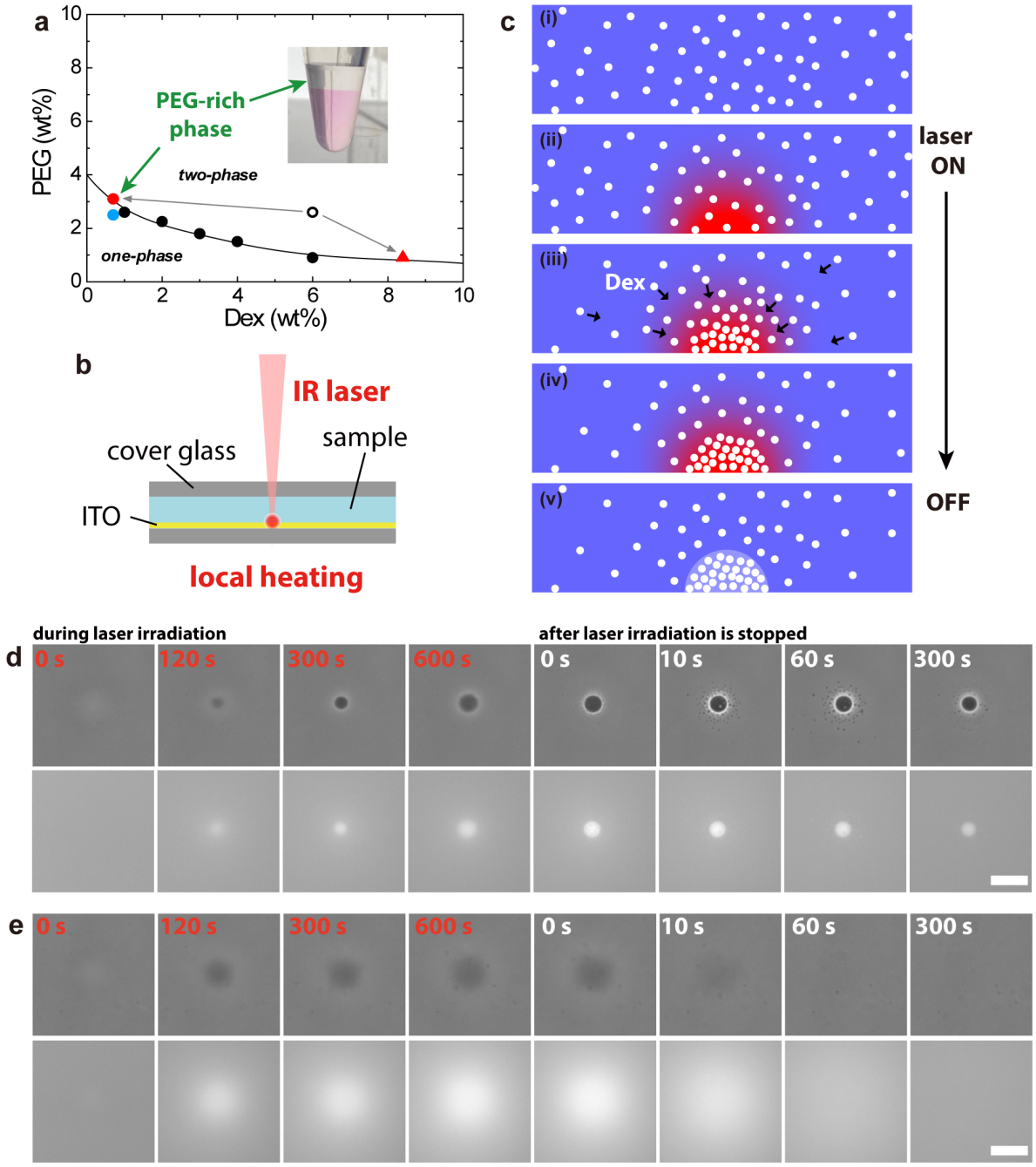

Fig. 1: Droplet generation induced by the Soret effect.

a, Phase diagram of the ATPS of Dextran (M_w = 5.5 × 10^5) and PEG (M_w = 3.5 × 10^4). The black circles are phase boundary obtained by visual observation. A sample was prepared with an initial composition of 6 wt.% and PEG 2.6wt.% (open circle) in a two-phase region. The mixture was phase-separated, and the composition of each phase is indicated by a red circle and triangle (See Methods). The upper PEG-rich phase of the phase-

separated mixture was used in droplet generation experiments. The black curve represents the coexisting curve. **b**, Experimental setup. The ITO coated on the cover glass absorbs laser light and causes local heating. **c**) Droplet generation process induced by the Soret effect. (See text.) Side view of the laser focus region. The white particles denote the dextran molecules. (i) Before laser irradiation. (ii) A temperature gradient occurs at the ITO surface when the laser irradiation is initiated. (iii) Dextran molecules enter the hot region. (iv) A dextran-rich domain formed. (v) The phase-separated droplets remain after the laser is switched off. **d**, Droplet generation process (Sample: upper phase of DEX 6 wt.% and PEG 2.6 wt.% including fluorescently labelled DEX 0.2 wt.%). (top) Phase contrast images. (Bottom) Fluorescence images of dextran. When the laser irradiation was initiated, a dark dextran-rich domain gradually appeared, and the droplet interface became sharp when the laser irradiation was stopped (see text). Successful droplet generation was observed only for the sample at the phase boundary. Scale bar = 20 μm. **e**, Cases in which no droplets were generated (DEX 0.7 wt.% and PEG 2.5 wt.% blue circle in the phase diagram). The sample composition was very close to that of **d** but only the behavior caused by the Soret effect was observed. Dextran collected by the Soret effect diffuses rapidly after the laser is switched off (local heating is removed). (top) Phase contrast images. (Bottom) Fluorescence images of dextran. Scale bar = 20 μm.

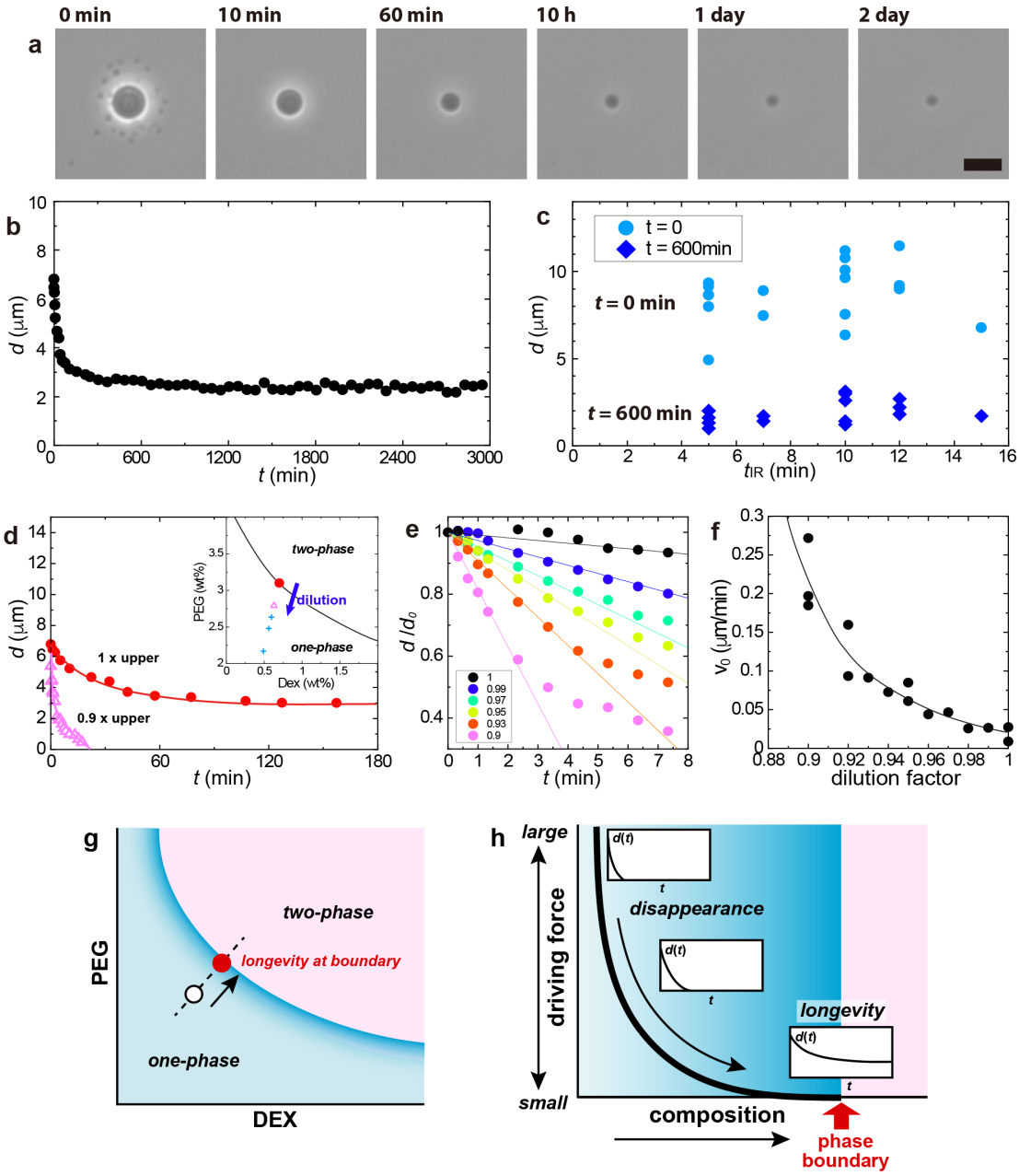

Fig. 2: Long-time droplet presence and its relationship with the distance to the coexisting curve.

a-c, Cases where the droplet generated in the sample on the coexisting curve sustains for a long time. The droplet was generated in the upper phase of 6 wt.% and PEG 2.6 wt.% (red circle in Fig. 1**a**). (**a**) Time evolution of phase-contrast images after the laser was switched off. (Laser irradiation time 10 min.) The number denotes the time elapsed after the laser was disabled. The droplets did not disappear and remained for more than two days. Scale bar = 10 μm. (**b**) Time evolution of droplet diameter. The value approached a finite value of

482 approximately 3 μm and converged. (**c**); Droplet diameters at t = 0 and 600 min plotted against the laser
483 irradiation time t_{IR}. **d-f**, Relationship between droplet generation behavior and distance to the coexisting curve
484 obtained by dilution experiments on the upper PEG-rich phase (see text). (**d**); Time evolution of droplet
485 diameter when the generated droplet disappears (pink triangles). This was attributed to the laser irradiation
486 experiment using a sample of the diluted upper PEG-rich phase with a dilution factor of 0.9. The long-time
487 presence achieved without dilution (dilution factor 1) is plotted for comparison (red circles). The solid curves
488 are visual guides. The inset shows the schematic illustration of dilution experiments. Red circle: upper PEG-
489 rich phase: sample on the coexisting curve (solid curve). Diluting the upper PEG-rich phase increases the
490 distance from the coexisting curve (a smaller dilution factor corresponds to being more distant from the
491 coexisting curve). The condition where the produced droplet disappeared (Pink triangle: dilution factor = 0.9).
492 Further dilution makes a condition where droplet generation is unsuccessful (Blue crosses). (**e**); Droplet
493 diameter in the initial regime. The diameter is normalized by the initial value at t = 0. The lines represent the
494 linear fits of the initial linear regime of time dependence. Numbers in the legend denote the dilution factor. (**f**);
495 Initial speed of droplet shrinkage obtained as the slope in the fit results in **e**. The speed decreases approaching
496 the coexisting curve: dilution factor =1. The solid curves represent visual guides. **g,h**, Schematic illustration
497 of the mechanism of longevity. (**g**); Schematic phase diagram of a DEX/PEG system. LIPS droplets generated
498 from the open circle inside the one-phase region disappear. When the initial sample is on the phase boundary
499 (red circle), LIPS droplet exhibits longevity. (**h**); The relationship between the behavior of a LIPS droplet (time
500 dependence of droplet diameter d(t) after switching off the laser) and the initial composition of the sample.
501 The longevity appears when the initial composition is approaching the phase boundary because of decreasing
502 the driving force to make the created LIPS droplet disappear.

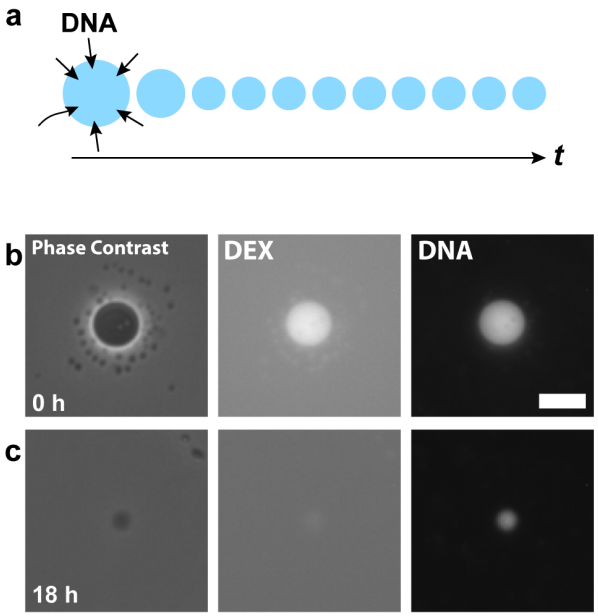

503

504 **Fig. 3: DNA enrichment in the LIPS droplet.**

505 **a**, Schematic illustration of the concept of long-time DNA enrichment in LIPS droplets. **b, c**, The droplet was

506 induced by laser irradiation for 5 min to the upper PEG-rich phase of DEX 6 wt.% and PEG 2.6wt.% + λ-DNA

507 (48,502 bp) 29 ng/μL. **b**, t = 0 h; **c**, t = 18 h after the laser is disabled. Phase-contrast image, fluorescent image

508 of dextran, and fluorescent image of the DNA observed by epifluorescence microscopy from left to right. The

509 droplet was visualized using a DNA intercalator and fluorescently labelled dextran. The DNA was successfully

510 incorporated into the generated dextran-rich droplet. Scale bar = 10 μm.

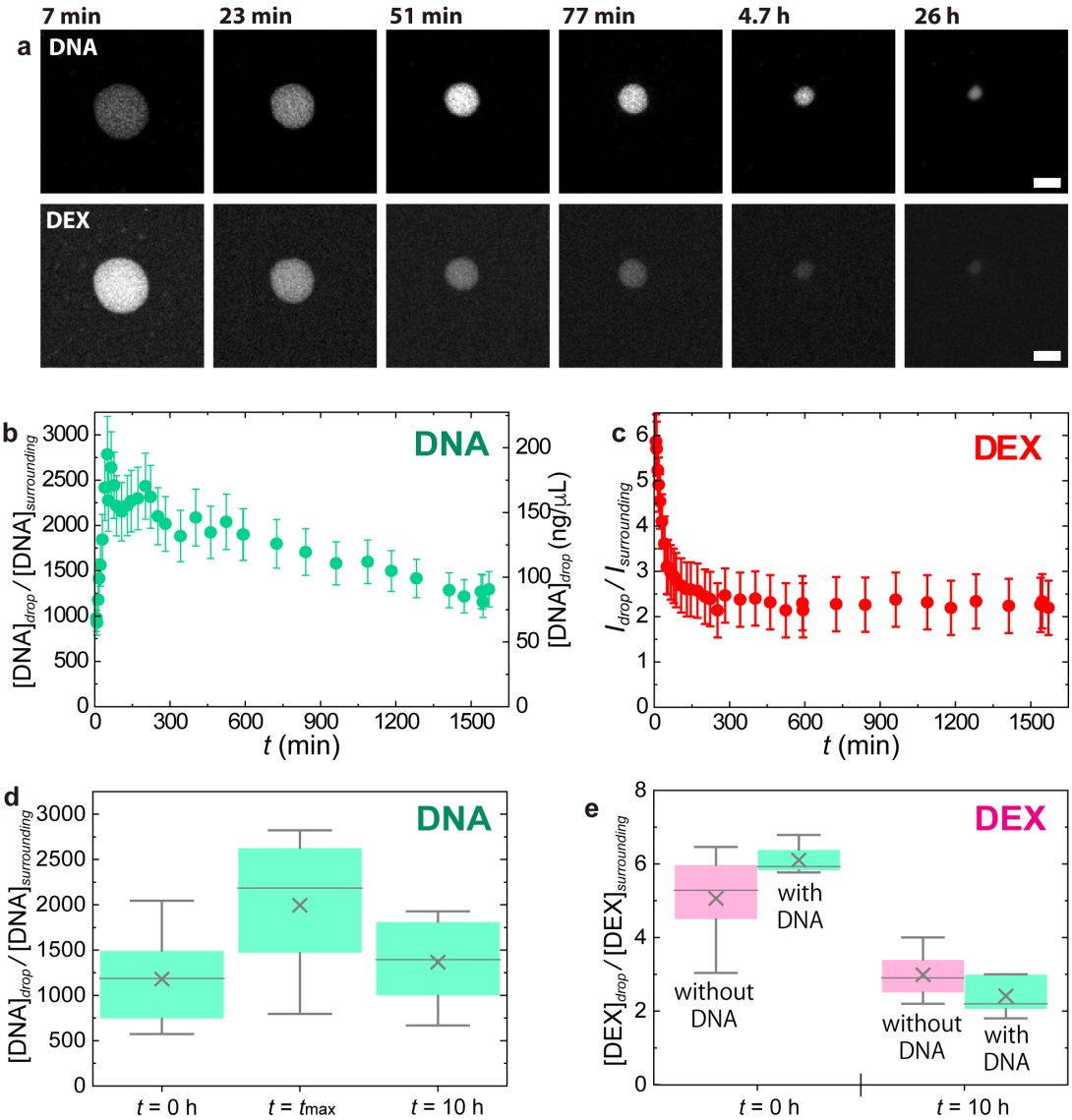

511

512 **Fig. 4: Time evolution of LIPS droplet observed by confocal measurements.**

513 The droplet was generated by laser irradiation for 12 min to the upper PEG-rich phase of DEX 6 wt.% and

514 PEG 2.6 wt.% + λ-DNA (48,502 bp) 29 ng/μL. **a,** Time-lapse image of a droplet visualized using a DNA

515 intercalator and fluorescently labelled dextran. The time in each image is the time after the termination of the

516 laser. Scale bar = 5 μm. **b**, DNA enrichment factor. Error bars are estimated from standard deviation in the

517 estimation of $c_{\text{surrounding}}$. **c**, Fluorescence intensity ratio of dextran. Error bars represent uncertainties from focal

518 positions. **d**, DNA enrichment factor at characteristic times. The time t_{max} denotes the time when the DNA

519 enrichment factor reaches its maximum value. It depends on the experiment (51 min for Fig. 4b) and is shown

520 in *SI Appendix*, Fig. S3. **e**, Dex intensity ratio at characteristic times in the case with and without DNA. In **d**

521 and **e**, 25–75 percentile (box), median (line), mean (cross), highest/lowest observations (whiskers).

522

523

524

525

526

527

528

529

530

531

532

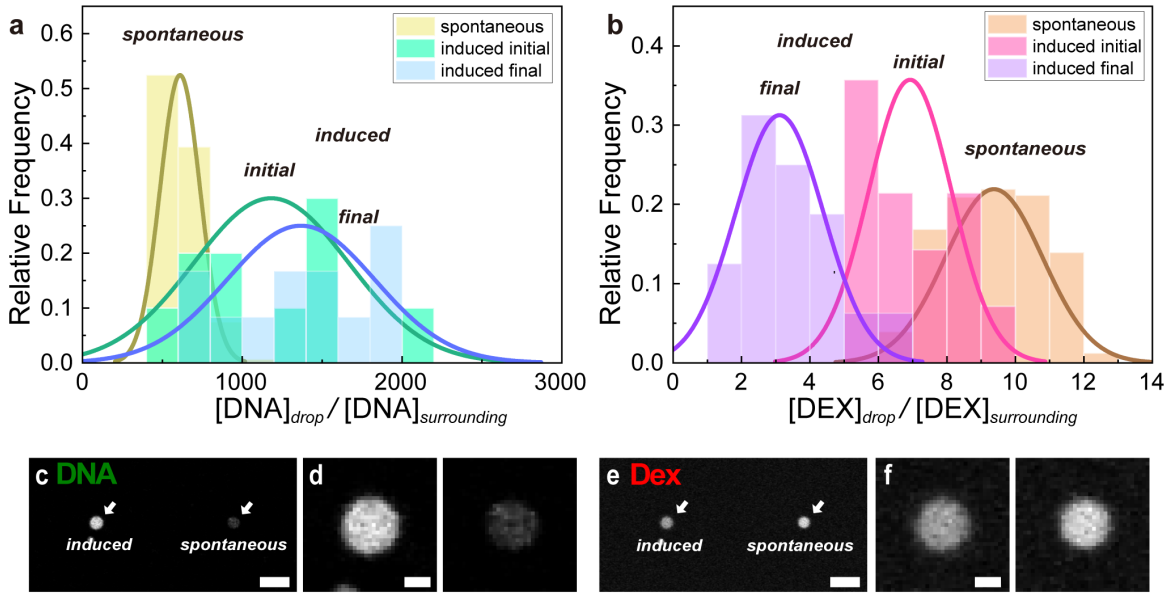

533 **Fig. 5: Comparison between LIPS droplets and the droplets by spontaneous phase separation. a-b**,
534 Histogram of the DNA enrichment factor and DEX concentration ratio of LIPS droplets and spontaneous
535 droplets. The initial ($t = 0$ h) and the final (long-time) values for LIPS droplets are displayed. The LIPS droplets
536 were generated from the upper PEG-rich phase of DEX 6 wt.% and PEG 2.6 wt.% with DNA (λ-DNA (48,502
537 bp) 29 ng/μL). Spontaneous droplets were produced from a two-phase mixture that has the same composition
538 as the one used for the preparation of the upper PEG-rich phase for LIPS experiments. **(a)**; Histogram of the
539 DNA enrichment factor. **(b)**; Histogram of concentration ratio of DEX between the droplet and the surrounding
540 phase. **c-f**, Confocal images of a LIPS droplet generated by laser irradiation for 7 min and a droplet generated
541 by spontaneous phase separation. The droplets were observed at t = 7 min after switching off the laser. **(c)**;
542 Confocal images of DNA. (left) LIPS droplet. (right) Droplet obtained by spontaneous phase separation. Scale
543 bar = 10 μm. **(d)**; Magnified image of droplets in Fig. 5c. Scale bar = 2 μm. **e**, Confocal image of DEX. Scale
544 bar = 10 μm. **(f)**; Magnified image of droplets in Fig. 5e. Scale bar = 2 μm.

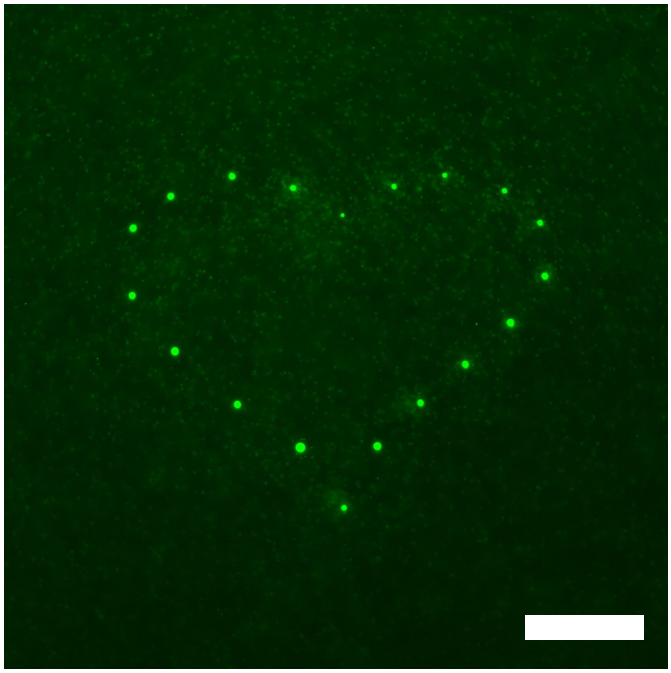

Fig. 6: Heart shape patterned by DNA-enriched droplets. Fluorescent image of λ-DNA (48,502 bp) observed by epifluorescence microscopy. Each droplet was generated by the laser irradiation of the sample for 5 min to the upper PEG-rich phase of DEX 6 wt.% and PEG 2.6 wt.% + λ-DNA (48,502 bp) 29 ng/µL. Scale bar = 100 µm.

References

1. A. A. Hyman, C. A. Weber, F. Jülicher, Liquid-Liquid Phase Separation in Biology. *Annu Rev Cell Dev Bi* **30**, 39–58 (2014).

2. Y. Shin, C. P. Brangwynne, Liquid phase condensation in cell physiology and disease. *Science* **357**, eaaf4382 (2017).

3. S. Alberti, A. Gladfelter, T. Mittag, Considerations and Challenges in Studying Liquid-Liquid Phase Separation and Biomolecular Condensates. *Cell* **176**, 419–434 (2019).

4. G. L. Dignon, R. B. Best, J. Mittal, Biomolecular Phase Separation: From Molecular Driving Forces to Macroscopic Properties. *Annu Rev Phys Chem* **71**, 53–75 (2020).

5. P.-Å. Albertsson, Partition of Proteins in Liquid Polymer–Polymer Two-Phase Systems. *Nature* **182**, 709–711 (1958).

6. C. D. Crowe, C. D. Keating, Liquid–liquid phase separation in artificial cells. *Interface Focus* **8**, 20180032 (2018).

7. H. Sakuta, *et al.*, Aqueous/Aqueous Micro Phase Separation: Construction of an Artificial Model of Cellular Assembly. *Front Chem* **7**, 44 (2019).

8. Y. Minagawa, S. Nakata, M. Date, Y. Ii, H. Noji, On-Chip Enrichment System for Digital Bioassay Based on Aqueous Two-Phase System. *Acs Nano* **17**, 212–220 (2023).

9. N. Nakatani, *et al.*, Specific Spatial Localization of Actin and DNA in a Water/Water Microdroplet: Self-Emergence of a Cell-Like Structure. *Chembiochem* **19**, 1370–1374 (2018).

10. V. P. Shanbhag, C. Axelsson, Hydrophobic Interaction Determined by Partition in Aqueous Two-Phase Systems. *Eur J Biochem* **60**, 17–22 (1975).

11. Y. Chao, H. C. Shum, Emerging aqueous two-phase systems: from fundamentals of interfaces to biomedical applications. *Chem Soc Rev* **49**, 114–142 (2020).

12. J. P. Frampton, *et al.*, Aqueous two-phase system patterning of detection antibody solutions for cross-reaction-free multiplex ELISA. *Sci. Rep.* **4**, 4878 (2014).

13. Q. Ma, *et al.*, Cell-Inspired All-Aqueous Microfluidics: From Intracellular Liquid–Liquid Phase Separation toward Advanced Biomaterials. *Adv. Sci.* **7**, 1903359 (2020).

14. Z. Xu, *et al.*, Photosynthetic hydrogen production by droplet-based microbial micro-reactors under aerobic conditions. *Nat. Commun.* **11**, 5985 (2020).

15. R. Mizuuchi, N. Ichihashi, Translation-coupled RNA replication and parasitic replicators in membrane-free compartments. *Chem. Commun.* **56**, 13453–13456 (2020).

16. J. P. Delville, C. Lalaude, E. Freysz, A. Ducasse, Phase separation and droplet nucleation induced by an optical piston. *Phys Rev E* **49**, 4145–4148 (1994).

17. J. P. Delville, C. Lalaude, A. Ducasse, Kinetics of laser-driven phase separation induced by a tightly focused wave in binary liquid mixtures. *Physica A Statistical Mech Appl* **262**, 40–68 (1999).

18. S.-A. Mukai, N. Magome, H. Kitahata, K. Yoshikawa, Liquid/liquid dynamic phase separation induced by a focused laser. *Appl Phys Lett* **83**, 2557–2559 (2003).

19. N. Kitamura, M. Yamada, S. Ishizaka, K. Konno, Laser-Induced Liquid-to-Droplet Extraction of Chlorophenol: Photothermal Phase Separation of Aqueous Triethylamine Solutions. *Anal Chem* **77**, 6055–6061 (2005).

20. Y. Tsuboi, M. Nishino, Y. Matsuo, K. Ijiro, N. Kitamura, Phase Separation of Aqueous Poly(vinyl methyl ether) Solutions Induced by the Photon Pressure of a Focused Near-Infrared Laser Beam. *B Chem Soc Jpn* **80**, 1926–1931 (2007).

21. A. Voit, A. Krekhov, W. Enge, L. Kramer, W. Köhler, Thermal Patterning of a Critical Polymer Blend. *Phys Rev Lett* **94**, 214501 (2005).

22. A. Voit, A. Krekhov, W. Köhler, Laser-induced structures in a polymer blend in the vicinity of the phase boundary. *Phys Rev E* **76**, 011808 (2007).

23. M. Shimizu, *et al.*, Space-selective phase separation inside a glass by controlling compositional distribution with femtosecond-laser irradiation. *Appl Phys* **100**, 1001–1005 (2010).

24. K. Yuyama, T. Sugiyama, H. Masuhara, Millimeter-Scale Dense Liquid Droplet Formation and Crystallization in Glycine Solution Induced by Photon Pressure. *J Phys Chem Lett* **1**, 1321–1325 (2010).

25. F. Walton, K. Wynne, Control over phase separation and nucleation using a laser-tweezing potential. *Nat Chem* **10**, 506–510 (2018).

26. F. Walton, K. Wynne, Using optical tweezing to control phase separation and nucleation near a liquid–liquid critical point. *Soft Matter* **15**, 8279–8289 (2019).

27. O. Y. Gowayed, *et al.*, Dynamic Light Scattering Study of a Laser-Induced Phase-Separated Droplet of Aqueous Glycine. *J Phys Chem B* **125**, 7828–7839 (2021).

28. M. Pavlovic, M. Antonietti, B. V. K. J. Schmidt, L. Zeininger, Responsive Janus and Cerberus emulsions via temperature-induced phase separation in aqueous polymer mixtures. *J Colloid Interf Sci* **575**, 88–95 (2020).

29. J. K. Platten, The Soret Effect: A Review of Recent Experimental Results. *J Appl Mech* **73**, 5–15 (2006).

30. D. Niether, S. Wiegand, Thermophoresis of biological and biocompatible compounds in aqueous solution. *J Phys Condens Matter* **31**, 503003 (2019).

31. R. Sugaya, B. A. Wolf, R. Kita, Thermal Diffusion of Dextran in Aqueous Solutions in the Absence and the Presence of Urea. *Biomacromolecules* **7**, 435–440 (2006).

32. E. Atefi, D. Fyffe, K. B. Kaylan, H. Tavana, Characterization of Aqueous Two-Phase Systems from Volume and Density Measurements. *J Chem Eng Data* **61**, 1531–1539 (2016).

33. S. Duhr, D. Braun, Why molecules move along a temperature gradient. *Proc National Acad Sci* **103**, 19678–19682 (2006).

34. Y. T. Maeda, A. Buguin, A. Libchaber, Thermal Separation: Interplay between the Soret Effect and Entropic Force Gradient. *Phys Rev Lett* **107**, 038301 (2011).

35. Y. T. Maeda, T. Tlusty, A. Libchaber, Effects of long DNA folding and small RNA stem–loop in thermophoresis. *Proc National Acad Sci* **109**, 17972–17977 (2012).

36. D. Braun, A. Libchaber, Trapping of DNA by Thermophoretic Depletion and Convection. *Phys. Rev. Lett.* **89**, 188103 (2002).

37. E. R. Dufresne, G. C. Spalding, M. T. Dearing, S. A. Sheets, D. G. Grier, Computer-generated holographic optical tweezer arrays. *Rev. Sci. Instrum.* **72**, 1810–1816 (2001).

38. X. Chen, *et al.*, Optothermally Programmable Liquids with Spatiotemporal Precision and Functional Complexity. *Adv. Mater.* **34**, e2205563 (2022).

39. A. Onuki, *Phase transition dynamics* (Cambridge University Press, 2002).

639 40. C. P. Brangwynne, *et al.*, Germline P Granules Are Liquid Droplets That Localize by Controlled
640 Dissolution/Condensation. *Science* **324**, 1729–1732 (2009).

641 41. D. Hnisz, K. Shrinivas, R. A. Young, A. K. Chakraborty, P. A. Sharp, A Phase Separation Model for
642 Transcriptional Control. *Cell* **169**, 13–23 (2017).

643 42. S. Boeynaems, *et al.*, Protein Phase Separation: A New Phase in Cell Biology. *Trends Cell Biol* **28**, 420–
644 435 (2018).

645 43. J. Agudo-Canalejo, *et al.*, Wetting regulates autophagy of phase-separated compartments and the cytosol.
646 *Nature* **591**, 142–146 (2021).

647 44. J. A. Morin, *et al.*, Sequence-dependent surface condensation of a pioneer transcription factor on DNA.
648 *Nat. Phys.* **18**, 271–276 (2022).

649 45. E. Jambon-Puillet, *et al.*, Phase-separated droplets swim to their dissolution. *Nat. Commun.* **15**, 3919
650 (2024).

651 46. T. Iwata, *et al.*, Liquid Droplet Formation and Facile Cytosolic Translocation of IgG in the Presence of
652 Attenuated Cationic Amphiphilic Lytic Peptides. *Angew. Chem. Int. Ed.* **60**, 19804–19812 (2021).

653 47. M. R. Helfrich, L. K. Mangeney-Slavin, M. S. Long, K. Y. Djoko, C. D. Keating, Aqueous Phase
654 Separation in Giant Vesicles. *J Am Chem Soc* **124**, 13374–13375 (2002).

655